



Microphysical Characteristics of Snowfall in Seoul, South Korea and Their Changes with Meteorological Conditions

Seong-Ho Hong¹ · Joohyun Lee² · Jong-Jin Baik¹

Received: 8 July 2024 / Revised: 26 September 2024 / Accepted: 4 November 2024
© The Author(s) under exclusive licence to Korean Meteorological Society and Springer Nature B.V. 2024

Abstract

In this study, the microphysical characteristics of snowfall in Seoul, South Korea and their changes with meteorological conditions are examined using about 6-year observation data from a Parsivel disdrometer. The snow particle size distribution (PSD) exhibits convex-down shapes, being better represented by gamma distributions than exponential distributions. As snowfall rate increases, the snow PSD broadens and its peak rises. The changes in gamma PSD parameters with snowfall rate differ between the mean PSD and 1-min PSDs. The volume-weighted mean diameter D_m much more rapidly increases with snowfall rate in comparison with D_m in Beijing, China and Pyeongchang, South Korea, suggesting the relative importance of aggregation in Seoul. 77% of snowfall in Seoul occurs when northwesterly blows at the 850-hPa level. This snowfall is associated with west-high/east-low pressure patterns, large air–sea temperature differences ($\sim 19^\circ\text{C}$), and shallow ($\leq 2.5 \text{ km}$) precipitation systems, suggesting a large contribution of sea-effect snowfall from the Yellow Sea. The northwesterly-type snowfall with lower temperatures ($\leq 25\text{th} \text{ percentile}$, COLD) and with higher temperatures ($\geq 75\text{th} \text{ percentile}$, WARM) at the 850-hPa level is compared in the same intensity range of $0.5\text{--}1 \text{ mm h}^{-1}$. Compared with the WARM snowfall, the COLD snowfall has relatively broad PSDs and less-rimmed snow particles. The COLD snowfall is associated with relatively large wind shear, small static stability, low temperatures of $-21 \text{ to } -9^\circ\text{C}$, and low humidity in the lower atmosphere, which is attributed to relatively strong northwesterly resulting in relatively strong cold and dry advection. This implies that enhanced aggregation by stronger turbulence and dendritic growths can contribute to the broader PSDs and that weakened riming for the lower temperatures might be associated with the less-rimmed snow particles.

Keywords Snow particle size distribution · Disdrometer · Meteorological conditions · Seoul · Sea-effect snowfall

1 Introduction

Snowfall is a characteristic form of precipitation in winter in mid- and high latitude regions (Adhikari et al. 2018; Kulie and Milani 2018). Snowfall in winter may exhibit less liquid-equivalent accumulated amounts than rainfall in other seasons, yet its impacts are hard to be overlooked. Snowfall can lead to traffic congestion and transport delays (Bardal and Jørgensen 2017; Taszarek et al. 2020; RWMP 2023), cause power outages (Cerrai et al. 2020; Souto et al. 2024), and damage social infrastructures (Noguchi and Fujii 2000;

Strauss et al. 2020; Wang et al. 2023). The annual economic losses due to natural disasters associated with snowfall are reported to reach millions to billions of dollars, on average, in several countries including USA, China, and South Korea (e.g., NBSC 2023; MOIS 2024; NCEI 2024). Snow-related disasters are well-reviewed in Shijin et al. (2022). In order to prevent or mitigate the damages resulting from snowfall, accurate predictions of snowfall type and amount are vital. However, large uncertainty and variability in the size distribution, riming degree, and shape of snow particles hinder accurate snowfall predictions, necessitating better understanding of snowfall.

In regions adjacent to a warm water body such as the sea or lake, a certain type of mesoscale snowfall can occur. When cold air traverses the warm water, sensible and latent heat fluxes from the water increase significantly due to a large air–water temperature difference (Markowski and Richardson 2010). The large heat and moisture transport

✉ Jong-Jin Baik
jjbaik@snu.ac.kr

¹ School of Earth and Environmental Sciences, Seoul National University, Seoul 08826, South Korea

² Department of Atmospheric Science, Kongju National University, Gongju 32588, South Korea

destabilizes and moistens the cold air. This can result in moist convection and snowfall which are called the sea- or lake-effect snowfall. This type of snowfall often features cloud bands or open cellular cloud patterns (e.g., Nizioł et al. 1995; Atkinson and Zhang 1996; Nakai et al. 2005) which manifest boundary-layer shallow convection. The precipitation systems associated with sea- or lake-effect snowfall are relatively shallow (e.g., Stewart et al. 1995; Kulie et al. 2016, 2021), compared with those associated with large-scale synoptically driven snowfall (e.g., Gehring et al. 2020; Pettersen et al. 2020). Sea- or lake-effect snowfall was reported in many regions such as the Great Lakes regions (e.g., Kulie et al. 2021), the East Sea (also known as the Sea of Japan) (e.g., Steenburgh and Nakai 2020), the Shandong Peninsula, China (e.g., Bao and Ren 2018), UK (e.g., Norris et al. 2013), and the Baltic Sea (e.g., Mazon et al. 2015).

Seoul, the capital of South Korea, is one of the largest cities in East Asia where ~10 million people reside, with a high density of ~16000 km⁻² (KOSIS 2024). Although Seoul and its surrounding regions, called the Seoul metropolitan area, are not representative heavy snowfall regions in South Korea such as the Yeongdong region and Honam region (Nam et al. 2014; Ho et al. 2023), the influence of snowfall can be significant in the light of highly concentrated population and congested traffic (Cha 2010; Son et al. 2013; Ahn et al.

2015; Lee et al. 2015). Seoul is located in the western part of South Korea, being close to the Yellow Sea (Fig. 1). The winter climate of Seoul is characterized by cold and dry conditions with winter mean temperature and relative humidity of −0.3 °C and 56.1%, respectively, during 1991–2020 (KMA 2024). These conditions are associated with the cold and dry winter monsoon, including prevailing northwest-erlies (Ha et al. 2012). As the cold air moving along the northwest-erlies traverses the relatively warm Yellow Sea, it brings about sea-effect snowfall in the western part of South Korea (e.g., Kang 2001; Jeong and Park 2013; Lee and Min 2018). According to the classification and analysis of 109 snowfall events in South Korea conducted by Cheong et al. (2006), the air mass transformation-type events (i.e., sea-effect snowfall events) are most frequent and produce snowfall mainly on the west coast of South Korea and the events of other three types associated with extratropical cyclones can produce snowfall over entire South Korea. This indicates that the sea effect as well as the influence of extratropical cyclones largely contributes to the snowfall in the western part of South Korea where Seoul is located.

The studies of snowfall in the Seoul metropolitan area are less than those of snowfall in the Yeongdong and Honam regions, and many of them mainly focused on synoptic analysis of heavy snowfall cases (e.g., Ha et al. 2001; Lee 2002a, b). Nevertheless, a few studies investigated mesoscale

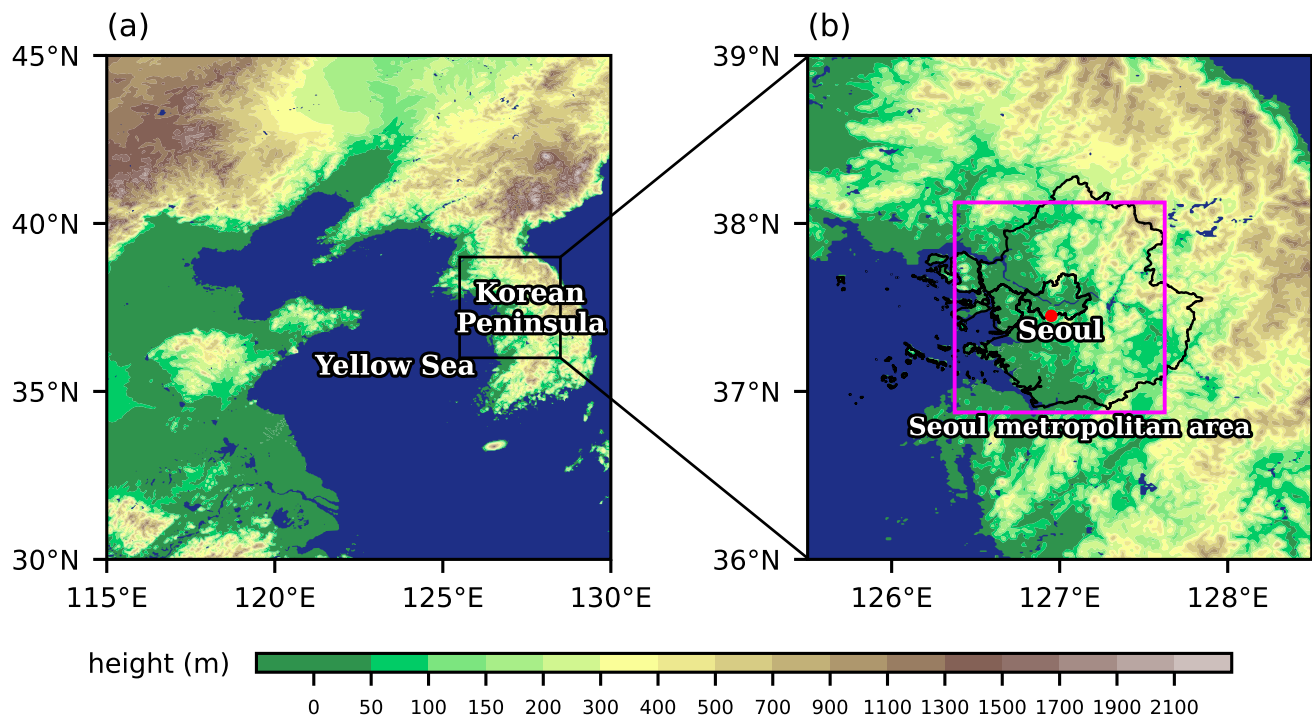


Fig. 1 (a) Land-sea distribution in and around the Korean Peninsula with terrain height (shades). (b) Location of the Seoul metropolitan area, including Seoul. In (b), the red dot denotes the location of

the Parsivel disdrometer and the pink box denotes the area used to average ERA5 850-hPa wind and temperature for analysis in subsection 3.2 (see the text)

or microphysical aspects of snowfall. Using Doppler radar and radiosonde observations, Yu and Kim (2005) examined the characteristics and development of cloud streets that produced heavy snowfall in the Seoul metropolitan area. They reported that the passage of a weak cold front with the expansion of the Siberian high leads to the cold advection below the height of ~ 1.3 km and the cloud streets are developed by the inflection point instability associated with large low-level wind shear. Kang and Kwon (2016) investigated the impacts of air-sea interaction on two snowfall events using numerical simulations with different heat and momentum exchange coefficients over the sea. They showed that the increase in heat exchange coefficient results in precipitation increases by destabilizing and moistening the atmosphere through increased sensible and latent heat fluxes. Allabakash et al. (2019) used a dual-polarization radar to investigate microphysical processes involved in a severe winter storm in the Seoul metropolitan area. They showed that the winter storm initially features depositional growths of dendrites and platelike crystals, subsequently generates heavy snowfall with intense aggregation, and produces large graupels with heavy riming later on.

Despite the importance of microphysical processes to snowfall, microphysical aspects of snowfall have been little investigated in the Seoul metropolitan area. The microphysical evolution of a winter storm is described in detail by Allabakash et al. (2019), but as they pointed out, this storm is an uncommon event producing large graupels in this region. To the authors' knowledge, general characteristics of snow particle size distribution (PSD) and their changes with meteorological conditions have not been investigated yet in the Seoul metropolitan area using long-term observations. This investigation not only enhances the understanding of the microphysical processes involved in the snowfall in this metropolitan city but also provides insights into the sea-effect snowfall associated with the Yellow Sea/Bohai Sea which affects several other East Asian regions such as Honam, South Korea; Shandong, China; and Hwanghae, North Korea.

This study examines the microphysical characteristics of snowfall in Seoul and their changes with meteorological conditions using disdrometer data over about 6 years. In Section 2, the datasets used in this study are explained. The results are provided with associated discussion in Section 3. In Section 4, a summary and conclusions of this study are given.

2 Datasets

This study uses snow particle observation data from the OTT Parsivel disdrometer (Tokay et al. 2014) installed at Seoul National University (37.45°N , 126.95°E) in Seoul

(Fig. 1b). The OTT Parsivel is a laser-based optical disdrometer, which measures the diameter and fall velocity of a hydrometeor particle using the area and duration of the shadow cast by the particle falling into a laser beam of 5.4 cm^3 ($18\text{ cm} \times 3\text{ cm} \times 0.1\text{ cm}$). The measured diameter and velocity are classified into 32 diameter bins ranging over $0\text{--}26\text{ mm}$ and 32 velocity bins ranging over $0\text{--}22.4\text{ m s}^{-1}$, respectively. Based on the classification, the particle is counted in 32×32 bins. These particle counts in 32×32 bins are saved every 1 min. For each of these 1-min data, the Parsivel assigns the precipitation type, which is drizzle, drizzle with rain, rain, rain and drizzle with snow, snow, snow grains, soft hail, or hail. The data with the precipitation type of "snow" are used in this study.

Several quality control procedures are applied to the disdrometer data. The data in the first two diameter bins are discarded due to the low signal-to-noise ratio (Tokay et al. 2014). The snow particles with fall velocities larger than 1.4 times the empirical raindrop fall velocity of Atlas et al. (1973) are excluded from the data (Kim et al. 2021), considering margin fallers and a reliable range of snow particle fall velocity. To avoid data subject to significant wind-induced errors (e.g., Nešpor et al. 2000), the 1-min data are retained only if the wind speed observed at the Parsivel location is smaller than 4 m s^{-1} (Brandes et al. 2007). After the quality control procedures mentioned above are applied, the data with snowfall rates $> 0.05\text{ mm h}^{-1}$ and with total particle counts ≥ 100 are used for analysis if they consecutively exist for at least 3 min (Thompson et al. 2015). The Parsivel data from 12 March 2018 to 19 February 2024 (~ 6 years) are used in this study, and among them, snow data with a length of 5111 min are left for analysis after the quality control procedures.

Various snow-related variables examined in this study are calculated using the 1-min disdrometer data. The snow PSD is obtained as follows:

$$N(D_i) = \sum_{j=1}^{32} \frac{n_{ij}}{A_i V_j \Delta t \Delta D_i} \quad (1)$$

Here, $N(D_i)$ ($\text{m}^{-3} \text{ mm}^{-1}$) is the number concentration of snow particles per unit volume per unit diameter interval in the i th diameter bin, D_i (mm) is the mid-value of the i th diameter bin, n_{ij} is the snow particle counts in the i th diameter bin and j th fall velocity bin, A_i (m^2) is the effective sampling area of the Parsivel for the i th diameter bin (Tokay et al. 2014), V_j (m s^{-1}) is the mid-value of the j th fall velocity bin, Δt (s) is the sampling interval of particle counts (i.e., 1 min), and ΔD_i (mm) is the width of the i th diameter bin. The snowfall rate S (mm h^{-1}) is calculated as the liquid water-equivalent intensity:

$$S = \frac{36 \times 10^{-4}}{\rho_w} \sum_{i=3}^{32} \sum_{j=1}^{32} \frac{\rho_s(D_i) \frac{\pi}{6} D_i^3 n_{ij}}{A_i \Delta t} \quad (2)$$

where ρ_w (g cm^{-3}) is the density of liquid water and ρ_s (g cm^{-3}) is the bulk density of snow. For $\rho_s(D)$, the empirical relationship between density and diameter obtained by Brandes et al. (2007) is used. The ice water content IWC (g m^{-3}) and equivalent radar reflectivity factor Z_e ($\text{mm}^6 \text{m}^{-3}$) (Löffler-Mang and Blahak 2001) are expressed as follows:

$$\begin{aligned} \text{IWC} &= \int \frac{\pi}{6} \rho_s D^3 N(D) dD \\ &\approx 10^{-3} \sum_{i=3}^{32} \frac{\pi}{6} \rho_s(D_i) D_i^3 N(D_i) \Delta D_i \end{aligned} \quad (3)$$

$$\begin{aligned} Z_e &= \frac{|K_I|^2}{\rho_I^2 |K_w|^2} \int \rho_s^2 D^6 N(D) dD \\ &\approx \frac{|K_I|^2}{\rho_I^2 |K_w|^2} \sum_{i=3}^{32} \{\rho_s(D_i)\}^2 D_i^6 N(D_i) \Delta D_i \end{aligned} \quad (4)$$

Here, $|K_I|^2$ and $|K_w|^2$ are the dielectric factors of ice and water (Löffler-Mang and Blahak 2001), respectively, and ρ_I (g cm^{-3}) is the density of ice.

The volume-weighted mean diameter D_m (mm) and generalized intercept parameter N_w ($\text{m}^{-3} \text{mm}^{-1}$) are the two PSD parameters that have been used to describe the PSD and to compare the characteristics of different PSD samples. They are calculated as follows:

$$D_m = \frac{M_4}{M_3} \quad (5)$$

$$N_w = \frac{4^4}{6} \left(\frac{M_3}{D_m^4} \right) \quad (6)$$

where M_n ($\text{m}^{-3} \text{mm}^n$) is the n th PSD moment which is calculated as

$$\begin{aligned} M_n &= \int D^n N(D) dD \\ &\approx \sum_{i=3}^{32} D_i^n N(D_i) \Delta D_i \end{aligned} \quad (7)$$

The total number concentration N_t (m^{-3}) is closely associated with the PSD peak and calculated as follows:

$$N_t = M_0 \quad (8)$$

The PSDs are often approximately represented using the exponential distribution function and gamma distribution function in remote sensing algorithms (e.g., Liao et al. 2014) and microphysics parameterizations (e.g., Hong et al. 2004; Morrison et al. 2009). These two distribution functions have the following forms:

$$N(D) = N_0 \exp(-\Lambda D) \quad (9)$$

$$N(D) = N_0 D^\mu \exp(-\Lambda D) \quad (10)$$

where N_0 is the intercept parameter ($\text{m}^{-3} \text{mm}^{-1}$, exponential PSD; $\text{m}^{-3} \text{mm}^{-\mu-1}$, gamma PSD), μ is the shape parameter, and Λ is the slope parameter (mm^{-1}). Examinations of the exponential and gamma PSD parameters using the observed PSDs could be valuable for practical applications as well as understanding of PSD characteristics. The N_0 and Λ of exponential PSD are calculated using M_2 and M_4 of the observed PSD (Zhang et al. 2008):

$$N_0 = \frac{M_2 \Lambda^3}{\Gamma(3)} \quad (11)$$

$$\Lambda = \left[\frac{M_2 \Gamma(5)}{M_4 \Gamma(3)} \right]^{\frac{1}{2}} \quad (12)$$

where Γ is the gamma function. The N_0 , μ , and Λ of gamma PSD are calculated using M_2 , M_4 , and M_6 of the observed PSD (Cao and Zhang 2009):

$$N_0 = \frac{M_2 \Lambda^{\mu+3}}{\Gamma(\mu+3)} \quad (13)$$

$$\Lambda = \left[\frac{M_2}{M_4} (\mu+3)(\mu+4) \right]^{\frac{1}{2}} \quad (14)$$

$$\mu = \frac{(7 - 11\eta) - (\eta^2 + 14\eta + 1)^{1/2}}{2(\eta - 1)} \quad (15)$$

where η is given by

$$\eta = \frac{M_4^2}{M_2 M_6} \quad (16)$$

In addition to the PSD data from the Parsivel, other observation and reanalysis data are used together for analysis. The 1-min near-surface wind and temperature observation data at the Parsivel location are used for the quality control procedure of the Parsivel data or for analysis. The fifth-generation European Centre for Medium-Range Weather Forecasts Reanalysis (ERA5) data with a temporal resolution of 1 h and a horizontal resolution of 0.25° (Hersbach et al. 2020) are used to examine synoptic conditions, vertical profiles of meteorological variables, and the vertical extension of snowfall systems. In this study, snow characteristics under different meteorological conditions are compared. To examine the statistical significance of the differences in snow characteristics, the Wilcoxon rank sum test is conducted using 30-min mean PSDs.

3 Results and Discussion

3.1 Snow Characteristics

In this subsection, the general characteristics of snow in Seoul are described. Figure 2 shows the monthly variations of snowfall frequency and relative frequencies of different precipitation types during cold season. In winter (December to February), snowfall occurs for an average of 7.6 h per month (Fig. 2a) which accounts for 87% of the frequency of solid precipitation (snow, soft hail, and hail) and 31% of the frequency of total precipitation in winter (Fig. 2b). The relative frequency of snowfall in Seoul (31%) is lower than those observed in Daegwallyeong (40%) and Mokpo (44%), South Korea (Cha and Yum 2021) which are located in the representative heavy snowfall regions (i.e., the Yeongdong and Honam regions). The remaining precipitation in Seoul is mostly comprised of liquid precipitation with a negligible contribution of

mixed-phase precipitation (liquid with snow) (Fig. 2b). The frequency of solid precipitation is largest in December (9.5 h), while its proportion to the total precipitation is largest in January (37%) (Fig. 2b) when the monthly mean temperature in Seoul is lowest. The frequency and proportion of snowfall are largest in February (8.2 h and 31%) (Fig. 2a and b). November and March exhibit considerably lower frequency (< 3 h) and lower proportion (< 9%) of snowfall than the winter months.

The mean snow PSDs with different snowfall rates in Seoul are depicted by solid lines in Fig. 3. The 1-min PSDs are classified into five S categories (i.e., $0.05 \text{ mm h}^{-1} < S \leq 0.2 \text{ mm h}^{-1}$, $0.2 \text{ mm h}^{-1} < S \leq 0.5 \text{ mm h}^{-1}$, $0.5 \text{ mm h}^{-1} < S \leq 1 \text{ mm h}^{-1}$, $1 \text{ mm h}^{-1} < S \leq 2 \text{ mm h}^{-1}$, and $2 \text{ mm h}^{-1} < S$) based on their 1-min snowfall rates, and then averaged. For all S categories, snow PSDs are characterized by the peak in $D = 0.5\text{--}1 \text{ mm}$ and the convex-down (i.e., super-exponential) shape over $D \geq 1 \text{ mm}$. This super-exponential shape has been reported from previous airborne or near-surface observations (e.g., Gordon and Marwitz 1984;

Fig. 2 (a) Monthly mean snowfall frequency and (b) relative frequencies of different precipitation types in each month of cold season

Figure 2 consists of two panels. Panel (a) is a line graph showing monthly mean snowfall frequency (hour month⁻¹) from November to March. The frequency starts at approximately 1.0 in November, peaks at about 8.0 in December, dips to around 6.8 in January, rises to about 8.2 in February, and then drops sharply to about 3.0 in March. Panel (b) is a stacked bar chart showing the relative frequency (%) of different precipitation types for each month. The categories are liquid (dark grey), liquid with snow (black), snow (light blue), and soft hail or hail (blue). The total relative frequency is highest in December (around 95%) and lowest in March (around 90%). The 'liquid' category is dominant in all months, peaking in December at approximately 65%.

Fig. 3 Mean snow PSDs (solid lines) and the corresponding (a) exponential and (b) gamma PSDs (dotted lines) with different S categories

Figure 3 consists of two panels, (a) and (b), showing particle size distributions (PSDs) on a log-linear scale. The y-axis is labeled $N(D) (\text{m}^{-3} \text{ mm}^{-1})$ and the x-axis is labeled $D (\text{mm})$. Both axes range from 10^{-1} to 10^4 . Panel (a) shows exponential PSDs, and panel (b) shows gamma PSDs. Five solid lines represent different snowfall rate categories (S): $0.05 < S \leq 0.2$ (yellow), $0.2 < S \leq 0.5$ (orange), $0.5 < S \leq 1$ (brown), $1 < S \leq 2$ (red), and $2 < S$ (dark red). Corresponding dotted lines show the exponential and gamma fits. All curves peak at $D \approx 1 \text{ mm}$ and decay rapidly as D increases, with higher S values showing steeper decay.

Korean Meteorological Society Springer

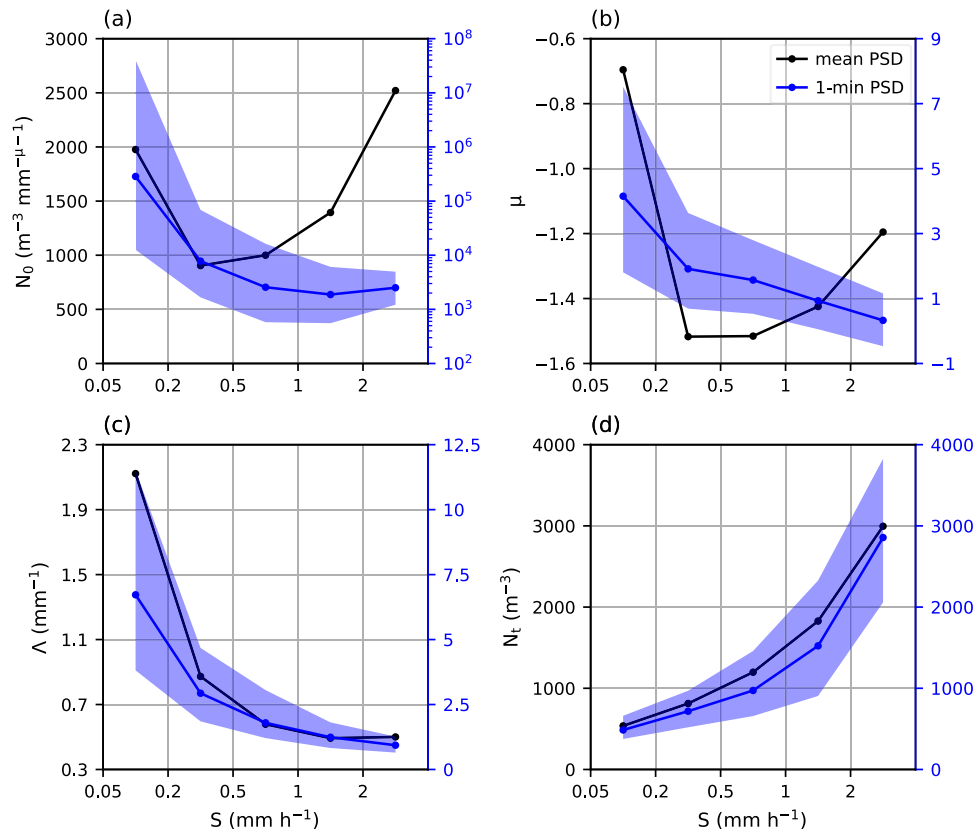
Brandes et al. 2007; Cha and Yum 2021; Shen et al. 2022). As the snowfall rate increases, the number concentrations of both small and large snow particles increase, which broadens the PSD and elevates its peak. This is consistent with the observations in Pyeongchang, South Korea (Yu et al. 2020) and Nanjing, China (Tao et al. 2021), while this differs from the observation in Beijing, China (Shen et al. 2022) where the number concentration increase is confined to the snow particles smaller than ~ 3.5 mm. When the mean PSDs are represented as the exponential PSDs (dotted lines in Fig. 3a), the numbers of relatively small and large snow particles are underestimated (e.g., $D < 2$ mm or $D > 8.5$ mm for $S > 2 \text{ mm h}^{-1}$) and the number of middle-sized snow particles (e.g., $2 \text{ mm} < D < 8.5 \text{ mm}$ for $S > 2 \text{ mm h}^{-1}$) is overestimated, because of their convex-down shapes. These underestimation and overestimation are significantly reduced when the mean PSDs are represented as the gamma PSDs (dotted lines in Fig. 3b).

To quantitatively characterize the variation of snow PSD with the snowfall rate, changes in the three gamma PSD parameters and N_t with increasing S are examined for the mean PSD and 1-min PSDs (Fig. 4). For the mean PSD (black lines), N_0 and μ substantially decrease when S increases from the $0.05\text{--}0.2 \text{ mm h}^{-1}$ range to $0.2\text{--}0.5 \text{ mm h}^{-1}$ range, and then increase with increasing S (Fig. 4a and b). This indicates that relationships between snowfall rate (a

bulk variable) and PSD parameters for light snowfall may differ from those for moderate or heavy snowfall. The negative μ reflects the super-exponential shape of the mean PSD (Fig. 4b). Λ exhibits a decreasing tendency with increasing S (Fig. 4c), reflecting the broadening of the mean PSD (Fig. 3). N_t increases with increasing S (Fig. 4d), which is in line with the elevating peak of the mean PSD (Fig. 3).

The gamma PSD parameters of 1-min PSDs (blue lines and shades) are distinguished from those of the mean PSD in terms of their variations with S , as well as their values (Fig. 4a–c). N_0 and μ of 1-min PSDs tend to keep decreasing with increasing S (Fig. 4a and b). For relatively light snowfall, N_0 of 1-min PSDs is generally 1–2 order larger than N_0 of the mean PSD (Fig. 4a). μ of 1-min PSDs is generally positive in contrast with μ of the mean PSD (Fig. 4b). The decreasing tendencies of N_0 and μ with increasing snowfall rate for short-time-averaged PSDs are also found in other observations (Brandes et al. 2007; Shen et al. 2022). Λ shows a decreasing tendency with increasing S , as in the mean PSD, yet exhibits much larger magnitudes (Fig. 4c). The differences in gamma PSD parameters between mean PSD and 1-min PSDs suggest that relationships between snowfall rate and gamma PSD parameters may depend on the temporal or spatial scales of sample size, implying that the parameterization of these parameters as a function of a bulk variable (e.g., snowfall rate) should be done with

Fig. 4 (a) Intercept parameter N_0 , (b) shape parameter μ , and (c) slope parameter Λ of gamma PSD and (d) total number concentration N_t for the mean snow PSDs (black lines) with different S categories. The median (blue lines) and interquartile range (blue shades) of the same parameters for 1-min snow PSDs are shown



caution. Meanwhile, N_t of 1-min PSDs is generally similar to that of the mean PSD (Fig. 4d), exhibiting an increasing tendency with increasing S as well.

The snow PSD characteristics can vary with the region, reflecting the differences in microphysical processes between regions. The snow PSD characteristics in Seoul are compared with those in different locations in East Asia using D_m and $\log_{10}N_w$ (Fig. 5). For each location, the pair of mean D_m and $\log_{10}N_w$ is denoted by a star. Seoul exhibits a larger mean D_m (3.05 mm) and a smaller mean $\log_{10}N_w$ (3.50) than Pyeongchang (Yu et al. 2020) and Beijing (Shen et al. 2022). Meanwhile, Nanjing (Pu et al. 2020) exhibits a larger mean D_m and a much smaller mean $\log_{10}N_w$ than the other locations. Aggregation likely leads to more effective growths in particle size than riming which results in the initial fill-in growth and later spherical growth (Heymsfield 1982; Seifert et al. 2019). In this regard, the regional differences in PSD characteristics suggest that aggregation plays a more important role in snowfall in Seoul compared with those in Pyeongchang and Beijing while it plays a less important role compared with that in Nanjing. Indeed, previous studies reported the importance of riming in snowfall in Pyeongchang and Beijing. Kim et al. (2021), who used the data from the same observation campaign as in Yu et al. (2020), showed that riming is dominant in the mountainous

locations in Pyeongchang. Shen et al. (2022) argued that the snow particles observed in Beijing are considered to be mainly small graupel particles. The results for Pyeongchang and Beijing in Fig. 5 are mostly obtained at mountainous locations where the terrain-induced updrafts can cause significant riming (Kusunoki et al. 2005).

Besides the mean D_m and $\log_{10}N_w$, their variations with the snowfall rate also differ between the locations (Fig. 5). The pairs of D_m and $\log_{10}N_w$ averaged for different S categories in each of Seoul, Pyeongchang, and Beijing are denoted by squares connected by a black line. For Nanjing, D_m and $\log_{10}N_w$ with different S categories are not available from Pu et al. (2020). When S is smaller than 0.5 mm h^{-1} , D_m in Seoul is smaller than or similar to those in Pyeongchang and Beijing. Meanwhile, D_m in Seoul is considerably larger than those in Pyeongchang and Beijing from S larger than 0.5 mm h^{-1} , since D_m in Seoul prominently increases with increasing S . The increase in D_m with increasing S is relatively small in Pyeongchang and is not apparent in Beijing. These results imply that the importance of aggregation more significantly increases with increasing snowfall intensity in Seoul in comparison with Pyeongchang and Beijing, leading to the larger mean particle size in Seoul. D_m and $\log_{10}N_w$ of snow PSDs have not been widely used to compare microphysical aspects between different regions, compared with those of raindrop size distribution. Further investigation of regional differences in D_m and $\log_{10}N_w$ and their associations with microphysical processes is needed for snow. The microphysical processes associated with snowfall in Seoul are further examined in the next subsection.

3.2 Changes in Snow Characteristics with Meteorological Conditions

The characteristics of snow particles are determined by microphysical processes, and these processes can be considerably affected by meteorological conditions. Winter in Seoul is dominated by the prevailing northwesterlies that bring cold and dry air. Most of the snowfall analyzed in this study is also associated with the northwesterlies; when the 1-min snowfall data are categorized according to the direction of 850-hPa wind averaged over the Seoul metropolitan area (pink box in Fig. 1b) during 3 h before the snowfall, the northwesterly-type (i.e., 270°–360°) snowfall accounts for 77% of the total data. In this subsection, the changes in snow characteristics are examined for the northwesterly-type snowfall which comprises the majority of snowfall in Seoul. Possible reasons for the changes in snow characteristics are also examined, with respect to the changes in meteorological conditions and microphysical processes. Hereafter, the word “northwesterly-type” is omitted for brevity.

Figure 6a and b show the fields of geopotential height, temperature, water vapor mixing ratio, and wind vector at

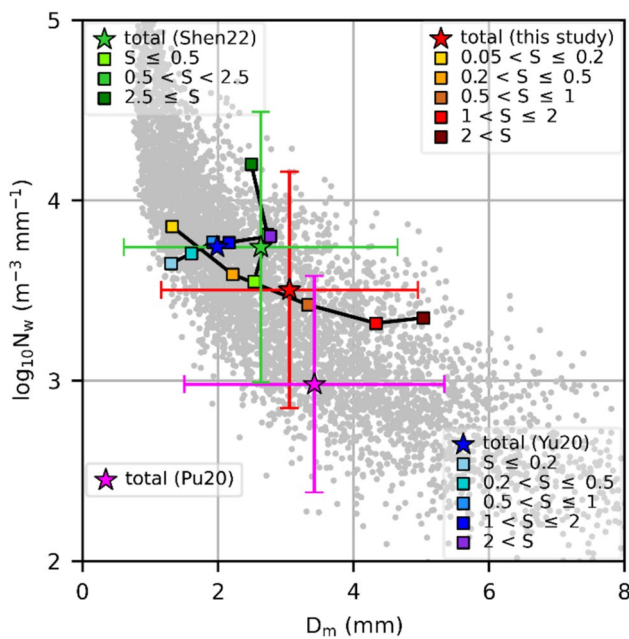


Fig. 5 Mean D_m and $\log_{10}N_w$ for total data (stars) and for different S categories (squares) at Seoul and other locations in East Asia: Pyeongchang, South Korea (Yu et al. 2020, Yu20); Beijing, China (Shen et al. 2022, Shen22); and Nanjing, China (Pu et al. 2020, Pu20). The ± 1 standard deviation ranges in total data are indicated by bars, if available. The scatterplot of D_m and $\log_{10}N_w$ for total data in Seoul is underlaid

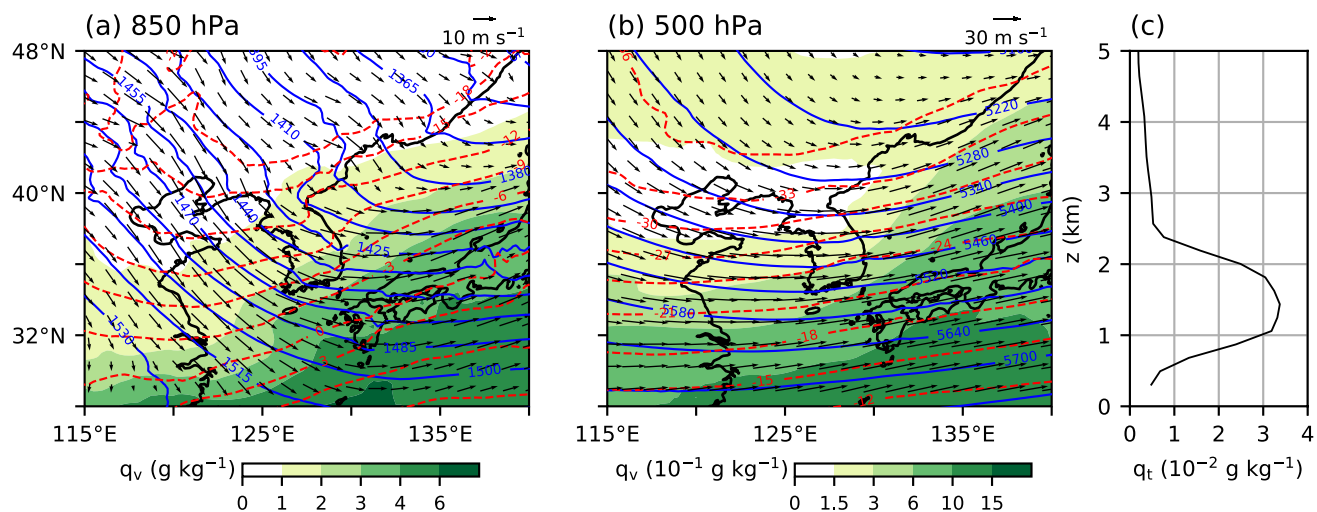


Fig. 6 Fields of geopotential height (blue solid lines), temperature (red dashed lines), water vapor mixing ratio (shades), and wind vector (arrows) at the (a) 850-hPa and (b) 500-hPa levels averaged over

3 h before the northwesterly-type snowfall. (c) Vertical profile of total hydrometeor mixing ratio averaged between 1 h before and after the northwesterly-type snowfall at the Parsivel location

the 850-hPa and 500-hPa levels averaged over 3 h before the snowfall. In the lower troposphere, the northeast–southwest pressure gradient prevails over the Yellow Sea and Korean Peninsula (Fig. 6a), which is attributed to the expanded Siberian high located west of the Korean Peninsula (i.e., over central and eastern China) and a low pressure located east of the Korean Peninsula (i.e., over Japan). The west-high/east-low pressure pattern has been reported for sea-effect snowfall events in South Korea (Cheong et al. 2006; Jeong and Park 2013; Lee and Min 2018). The pressure gradient results in prevalent geostrophic northwesterlies ($\sim 12 \text{ m s}^{-1}$) that bring cold and dry continental air toward the Korean Peninsula (Fig. 6a). In the middle troposphere, the monsoon trough is developed over Northeast Asia with strong geostrophic westerlies ($\sim 33 \text{ m s}^{-1}$) (Fig. 6b). Associated with the cold advection by the northwesterlies, the temperature difference between the air at the 850 hPa and the Yellow Sea reaches $\sim 19^\circ\text{C}$. This large air–water temperature difference exceeding 13°C can induce sea- or lake-effect snowfall (e.g., Niziol 1987; Bao and Ren 2018). The vertical profile of total hydrometeor mixing ratio averaged between 1 h before and after the snowfall shows that the precipitation systems associated with the snowfall are generally shallow ($< 2.5 \text{ km}$) (Fig. 6c). This is consistent with the clouds associated with lake-effect snowfall (Barthold and Kristovich 2011; Kulie et al. 2016; Pettersen et al. 2020). The maximum total hydrometeor mixing ratio is found at $z \sim 1.5 \text{ km}$ (Fig. 6c). The results from Fig. 6 suggest that the considered snowfall events are mainly associated with sea-effect snowfall.

The air temperature in the lower troposphere is regarded as an important factor to sea-effect snowfall, since its contrast to the sea surface temperature is closely linked with

the intensity of shallow convection over the sea. To examine snow characteristics for meteorological conditions with different low-level temperatures, the mean snow PSDs for lower low-level temperatures ($\leq 25\text{th}$ percentile, blue solid line) and higher low-level temperatures ($\geq 75\text{th}$ percentile, black solid line) are plotted in Fig. 7a. For this, the 850-hPa temperature averaged over the area in the pink box in Fig. 1b between 1 h before and after the snowfall is used. The 25th and 75th percentiles of the 850-hPa temperature are -16.6 and -8.1°C , respectively. Compared with the snowfall for higher temperatures, the snowfall for lower temperatures exhibits a relatively large S with relatively large number of snow particles and wide PSD. The mean D_m is larger for lower temperatures (3.21 mm) than for higher temperatures (2.78 mm). The relatively large S could be associated with a relatively large air–sea temperature difference for lower temperatures ($\sim 27^\circ\text{C}$), compared with that for higher temperatures ($\sim 13^\circ\text{C}$). The larger air–sea temperature difference can lead to enhanced shallow convection and more intense snowfall. Interestingly, the difference in snow PSD is found, even among the snowfall with similar intensity. Even when only the snowfall with S from 0.5 to 1.0 mm h^{-1} is considered, the snowfall has a broader PSD for lower temperatures (blue dotted line) than for higher temperatures (black dotted line). The mean $\log_{10}N(D)$ of large snow particles with diameters being 5–10 mm is statistically significantly ($p < 0.01$) larger for lower temperatures than for higher temperatures. Note that the mean S for lower temperatures and that for higher temperatures (0.71 and 0.73 mm h^{-1}) are very similar to each other. This implies possible changes in microphysical processes, besides the enhanced convection. Hereafter, among the snowfall with S from 0.5 to 1.0 mm h^{-1} ,

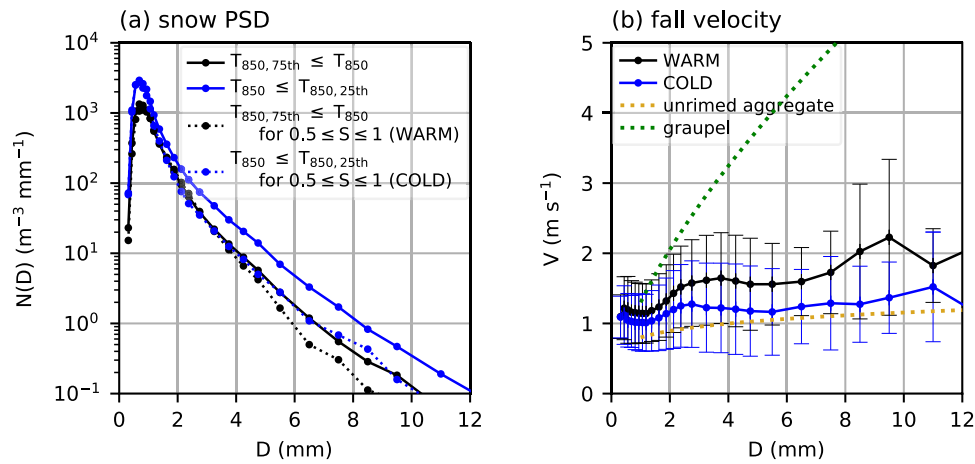


Fig. 7 (a) Mean snow PSDs of the northwesterly-type snowfall for lower low-level temperatures (≤ 25 th percentile) (blue solid line) and for higher low-level temperatures (≥ 75 th percentile) (black solid line). The same mean PSDs but for the northwesterly-type snowfall with S from 0.5 to 1.0 mm h^{-1} (i.e., the COLD and WARM snowfall) are depicted by blue and black dotted lines. (b) Mean fall velocities

of snow particles for the COLD snowfall (blue solid line) and for the WARM snowfall (black solid line) as a function of diameter. The ± 1 standard deviation ranges of fall velocities for the COLD and WARM snowfall are indicated by bars. The empirical fall velocities of lump graupel and unrimed aggregate obtained by Locatelli and Hobbs (1974) are depicted by green and yellow dotted lines, respectively

the snowfall for lower temperatures (≤ 25 th percentile) is called the COLD snowfall and the snowfall for higher temperatures (≥ 75 th percentile) is called the WARM snowfall. The 25th and 75th percentiles of the 850-hPa temperature for the snowfall with S from 0.5 to 1.0 mm h^{-1} are -17.5 and -8.3 $^{\circ}\text{C}$, respectively.

In addition to the snow PSD, the riming degree of snow particles differs between meteorological conditions with lower temperatures and those with higher temperatures. Figure 7b shows the snow particle fall velocities averaged for the COLD snowfall and for the WARM snowfall as a function of diameter. The fall velocity of snow particles has been used to estimate the riming degree by many studies (e.g., Zhang et al. 2011; Bukovčić et al. 2018; Shen et al. 2022), since it tends to increase with increasing degree of riming (e.g., Locatelli and Hobbs 1974; Brandes et al. 2008). For relatively large particles ($D > 5$ mm), the fall velocity of particles for the COLD snowfall is close to that of aggregates. Meanwhile, the fall velocity of particles for the WARM snowfall considerably deviates from that of aggregates, being larger than the fall velocity of particles for the COLD snowfall. The fall velocity averaged over the entire diameter range is statistically significantly ($p < 0.01$) smaller for the COLD snowfall than for the WARM snowfall. This suggests that the snow particles for the COLD snowfall are less rimed than those for the WARM snowfall, which implies possible changes in microphysical processes.

To understand the difference in snow characteristics, the synoptic conditions are compared between the COLD and WARM snowfall. Figure 8 shows the synoptic fields at the 850-hPa level averaged over 3 h before the COLD snowfall

and the WARM snowfall. The pressure patterns for both the COLD and WARM snowfall feature a relatively high pressure over central and eastern China and a relatively low pressure over Japan, as in Fig. 6a. However, these high and low pressures are pronounced and much strong for the COLD snowfall, thereby resulting in much large magnitude of pressure gradient over the Korean Peninsula. This produces much stronger geostrophic northwesterlies in the lower troposphere for the COLD snowfall ($\sim 15 \text{ m s}^{-1}$) than for the WARM snowfall ($\sim 8 \text{ m s}^{-1}$), resulting in a stronger cold and dry advection for the COLD snowfall. The pressure patterns in the middle troposphere for the COLD and WARM snowfall are qualitatively similar to the pattern shown in Fig. 6b, while the magnitude of north-south pressure gradient is much larger for the COLD snowfall than for the WARM snowfall (figure not shown). Hence, the mid-level geostrophic westerlies are stronger for the COLD snowfall than for the WARM snowfall.

To examine the difference in meteorological conditions, the vertical profiles of relative humidity with respect to liquid water, temperature, equivalent potential temperature, and magnitude of vertical wind shear averaged between 1 h before and after the COLD snowfall and the WARM snowfall at the Parsivel location are plotted (Fig. 9). The relative humidity below $z = 2$ km for the COLD snowfall is 24% lower than that for the WARM snowfall (Fig. 9a) due to the stronger dry advection associated with the stronger northwesterlies for the COLD snowfall (Fig. 8). The temperature below $z = 2$ km for the COLD snowfall ranges from -21 to -9 $^{\circ}\text{C}$, being much lower (11 $^{\circ}\text{C}$ on average) than that for the WARM snowfall which ranges from -7 to

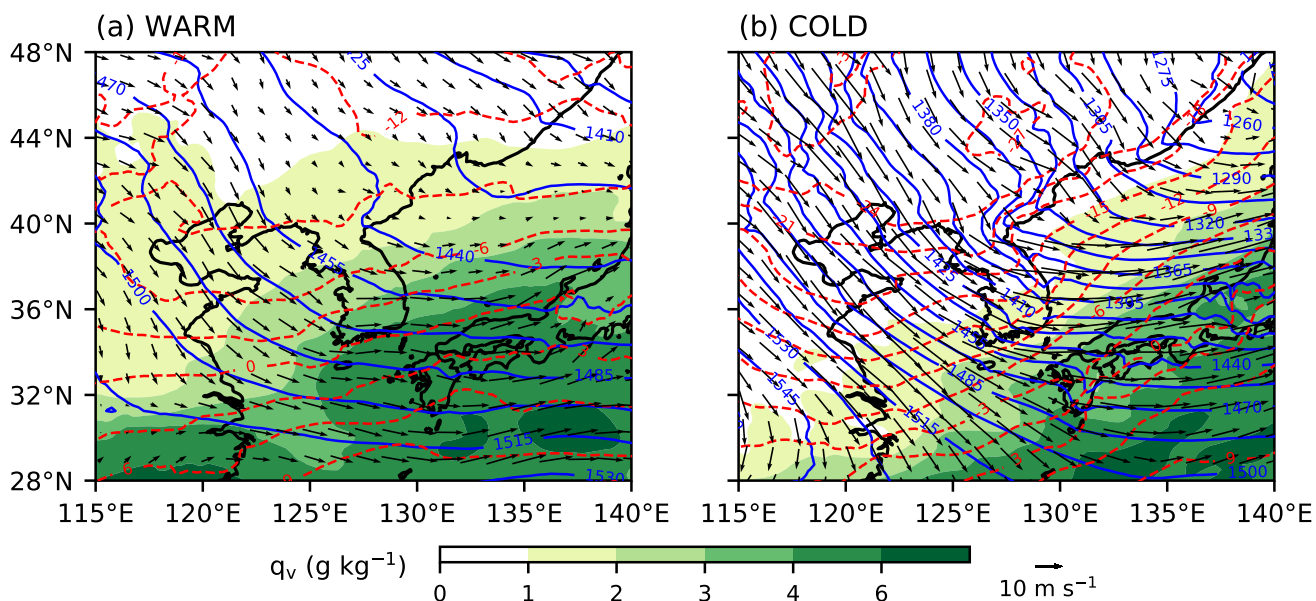


Fig. 8 As in Fig. 6a, but for (a) the WARM snowfall and for (b) the COLD snowfall

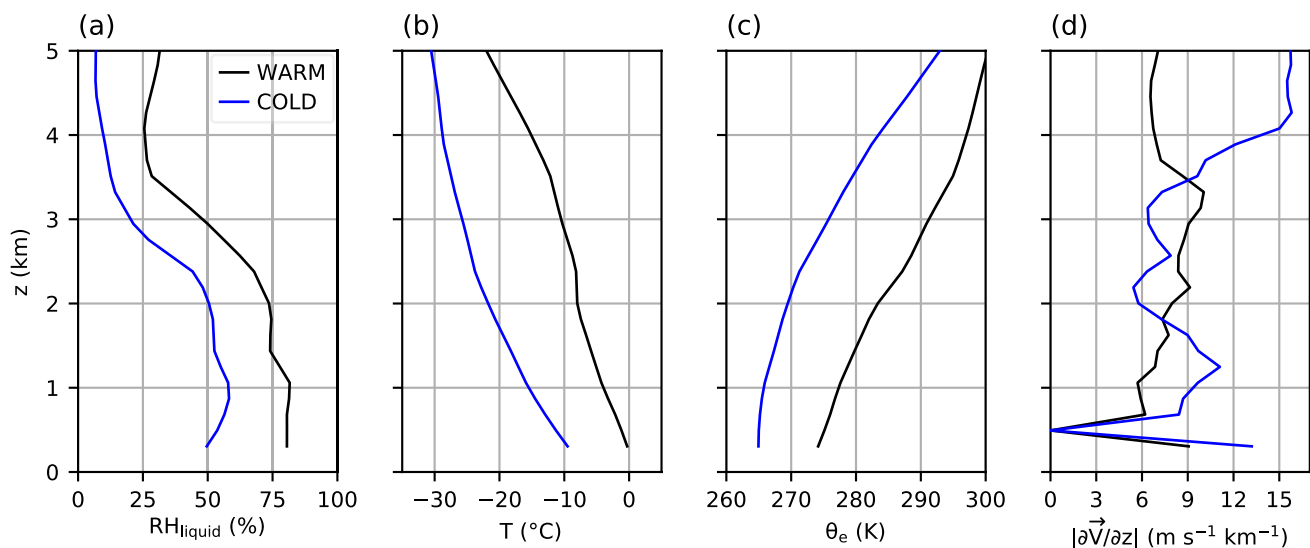


Fig. 9 Vertical profiles of (a) relative humidity with respect to liquid water, (b) temperature, (c) equivalent potential temperature, and (d) magnitude of vertical wind shear averaged between 1 h before and

after the COLD snowfall (blue lines) and the WARM snowfall (black lines) at the Parsivel location

0 °C (Fig. 9b). Previous studies reported that the amount of supercooled liquid water decreases with decreasing temperature (Korolev et al. 2003; Pinsky et al. 2015). The lower temperature for the COLD snowfall implies that shortages of supercooled liquid water might contribute to a weakening of riming, leading to the less-rimed snow particles in the COLD snowfall. Similarly, a long-term radar observation study by Kneifel and Moisseev (2020) found that riming less occurs at lower temperatures. They suggested that the

temperature dependence of riming is likely related to the temperature dependence of supercooled liquid water. Further investigation regarding the weaker riming associated with colder conditions for the snowfall in Seoul is needed.

Besides the humidity and temperature, the low-level stability and vertical wind shear also differ between the COLD and WARM snowfall (Fig. 9c and d). The difference in equivalent potential temperature between $z=0.3$ and 2 km for the COLD snowfall (4.5 K) is about half of that for the WARM snowfall

(9.2 K) (Fig. 9c). This is qualitatively consistent with the larger air-sea temperature difference for the COLD snowfall which is attributed to the stronger cold advection (Fig. 8). Moreover, the magnitude of vertical wind shear below $z = 1.8$ km for the COLD snowfall is generally larger (up to $4.2 \text{ m s}^{-1} \text{ km}^{-1}$) than that for the WARM snowfall (Fig. 9d), which is mainly attributed to the stronger low-level northwesterlies for the COLD snowfall (Fig. 8). The statically less stable and more strongly sheared conditions suggest stronger turbulence in the lower troposphere for the COLD snowfall. Turbulence enhances aggregation by increasing the number of collisions between snow particles (Pinsky and Khain 1998; Aikins et al. 2016; Pettersen et al. 2020). These suggest that enhanced aggregation associated with relatively strong turbulence may contribute to the relatively broad PSD of the COLD snowfall.

The range of low-level temperature for the COLD snowfall (i.e., from -21 to -9°C , Fig. 9b) largely overlaps with the temperature range of the dendritic growth zone where ice crystals tend to depositionally grow into dendrites and platelike crystals (e.g., Libbrecht 2005). Dendrites can be favorable for aggregation, since they increase the likelihood of entanglement after the collision (e.g., Rauber 1987). The range of low-level temperature for the COLD snowfall implies that more dendritic shapes of snow particles may further facilitate aggregation and hence contribute to the relatively broad PSD of the COLD snowfall.

Cha and Yum (2021) examined the changes in snow PSD with near-surface weather conditions using disdrometer data observed in Daegwallyeong and Mokpo, South Korea over about 2 years. They found that the number of large snow particles is relatively large when temperature is relatively low or wind speed is relatively large. These changes in snow PSD seem qualitatively in line with those found in Seoul in that the snow PSD in Seoul is relatively broad for the COLD snowfall which is associated with relatively low temperatures and large wind speeds near the surface (not shown). Meanwhile, the changes in PSD with meteorological conditions found in this study and Cha and Yum (2021) are different from those observed in Colorado, USA (Brandes et al. 2007) where the snow particle size shows an increasing tendency with increasing near-surface temperature. Winter climates and main snowfall systems differ depending on the region, which may lead to different associations between meteorological conditions and important microphysical processes. Further investigation of regional differences in relationships between snow PSDs and meteorological conditions is needed across various regions.

3.3 Quantitative Relationships Between Snow Parameters

Remote sensing algorithms and microphysics parameterizations assume various relations between hydrometeo-

parameters, and the adequacy of the relations is important to the quantitative precipitation estimation and forecast. In this subsection, several relations between snow parameters in Seoul are examined and compared with those obtained from other locations. Figure 10a shows the scatterplot of Λ versus μ in Seoul and the second-order polynomial fits of $\Lambda-\mu$ relations in Seoul and other locations. A $\Lambda-\mu$ relation enables the retrieval of three-parameter gamma PSD when only two PSD moments are available (Zhang et al. 2001; Vivekanandan et al. 2004). All relations shown in Fig. 10 are listed in Table 1. μ shows an increasing tendency with increasing Λ , consistent with previous studies (e.g., Brandes et al. 2007; Lee et al. 2022). Λ and μ for relatively heavy snowfall are concentrated near the origin at $(0, 0)$, and those for relatively light snowfall are scattered over a relatively wide range. When Λ is larger than 20 mm^{-1} , the $\Lambda-\mu$ relation in Seoul shows a large deviation from those in Beijing (Shen et al. 2022) and Colorado (Brandes et al. 2007). However, the snowfall with Λ larger than 20 mm^{-1} accounts for only a negligible portion, even for the light snowfall with $S \leq 0.5 \text{ mm h}^{-1}$ (3%). When Λ is smaller than 20 mm^{-1} , the $\Lambda-\mu$ relations in Seoul, Beijing, and Colorado are overall similar but the relation in Seoul is closer to the relation in Colorado than to the relation in Beijing.

Z_e-S and $Z_e-\text{IWC}$ relations allow estimating snowfall intensity and the amount of ice water in clouds from observed radar reflectivity. Figure 10b and c show the scatterplots of Z_e versus S and Z_e versus IWC in Seoul and the Z_e-S and $Z_e-\text{IWC}$ relations in Seoul and other locations. To reduce the overrepresentation of observations concentrated in a narrow Z_e range, the total Z_e range of 1-min data is divided into 20 intervals and the medians of S and IWC in each interval are used to obtain power law fits. Here, only the 1-min snowfall data with near-surface temperatures lower than 0°C are used to avoid wet snow (Shen et al. 2022). The exponent of Z_e-S relation in Seoul (0.42) is smaller than those in Järvenpää, Finland obtained by Huang et al. (2015) (0.61 and 0.69); Oklahoma, USA obtained by Buković et al. (2018) (0.64); and Beijing obtained by Shen et al. (2022) (0.78) (Fig. 10b and Table 1). Meanwhile, the exponent obtained in Seoul is similar to that obtained from airborne observations of Heymsfield et al. (2016) (0.37). Compared with the relation in Oklahoma, the relation in Seoul yields a relatively small Z_e for light and moderate snowfall ($< 2.2 \text{ mm h}^{-1}$) (Fig. 10b). Compared with the relation in Beijing, the relation in Seoul yields a relatively small Z_e for light snowfall ($< 0.3 \text{ mm h}^{-1}$) while it yields a relatively high Z_e for moderate and heavy snowfall. The difference in Z_e-S relation between Seoul and Beijing is possibly attributed to the relatively small particle size of light snowfall and relatively large particle size of moderate and heavy snowfall in Seoul, compared with Beijing, as shown by the mean D_m with different S categories (Fig. 5). This indicates that

Fig. 10 (a) Scatterplot of Λ versus μ in Seoul. Each dot is colored according to S . The second-order polynomial fits of $\Lambda-\mu$ relations in Seoul and other locations are depicted by different lines. Scatterplots of (b) Z_e versus S and (c) Z_e versus IWC in Seoul. The power-law fits of Z_e-S and Z_e-IWC relations in Seoul and other locations are depicted by different lines. The medians of S and IWC in each Z_e interval are indicated with dark gray lines with dots

an appropriate Z_e-S relation differs depending on the PSD characteristics which are influenced by winter climates and snowfall mechanisms in the region of interest.

The exponent of Z_e -IWC relation obtained in Seoul (0.45) is smaller than that in Oklahoma obtained by Bukovčić et al. (2018) (0.61), while it is close to that obtained from airborne observations of Heymsfield et al. (2016) (0.42) (Fig. 10c and Table 1). This is similar to the case of Z_e-S relation. The relation in Seoul yields a smaller Z_e than that in Oklahoma for small and middle IWC (Fig. 10c). Nonetheless, the two relations yield a similar Z_e for large IWC. An IWC-S relation is useful when only one of the Z_e-S and Z_e -IWC relations is available. By combining the Z_e -IWC relation with the Z_e-S relation in Seoul, the IWC-S relation in Seoul is obtained ($S=3.14 \text{ IWC}^{0.93}$). The IWC-S relation in Seoul exhibits a smaller coefficient and a smaller exponent than that in Pyeongchang ($S=7.61 \text{ IWC}^{1.26}$) obtained by Yu et al. (2020). It is rather closer to the relation obtained by Heymsfield et al. (2016) ($S=4.07 \text{ IWC}^{1.17}$) despite the relative proximity to Pyeongchang.

4 Summary and Conclusions

This study examines the snow characteristics in Seoul and their changes with meteorological conditions. For this, disdrometer observation data over about 6 years in Seoul are used. As the snowfall rate increases, the peak of snow PSD is elevated and the width of snow PSD increases. Regardless of the snowfall rate, the snow PSD exhibits a super-exponential shape over $D \geq 1 \text{ mm}$. The N_0 , μ , and Λ values and their variations with the snowfall rate show differences between the mean PSD and 1-min PSDs. Compared with Pyeongchang and Beijing, Seoul is characterized by relatively large D_m , small $\log_{10} N_w$, and large increase in D_m with increasing snowfall rate. This suggests that aggregation may play a more important role in Seoul than in Pyeongchang and Beijing.

77% of snowfall frequency in Seoul is associated with low-level northwesterlies resulting from west-high/east-low pressure patterns. This snowfall is characterized by a large air-sea temperature difference of, on average, 19°C and shallow precipitation systems, which indicates a large contribution of sea-effect snowfall from the Yellow Sea. Among the northwesterly-type snowfall with snowfall rates of 0.5 to 1 mm h^{-1} , the snowfall for lower low-level temperatures

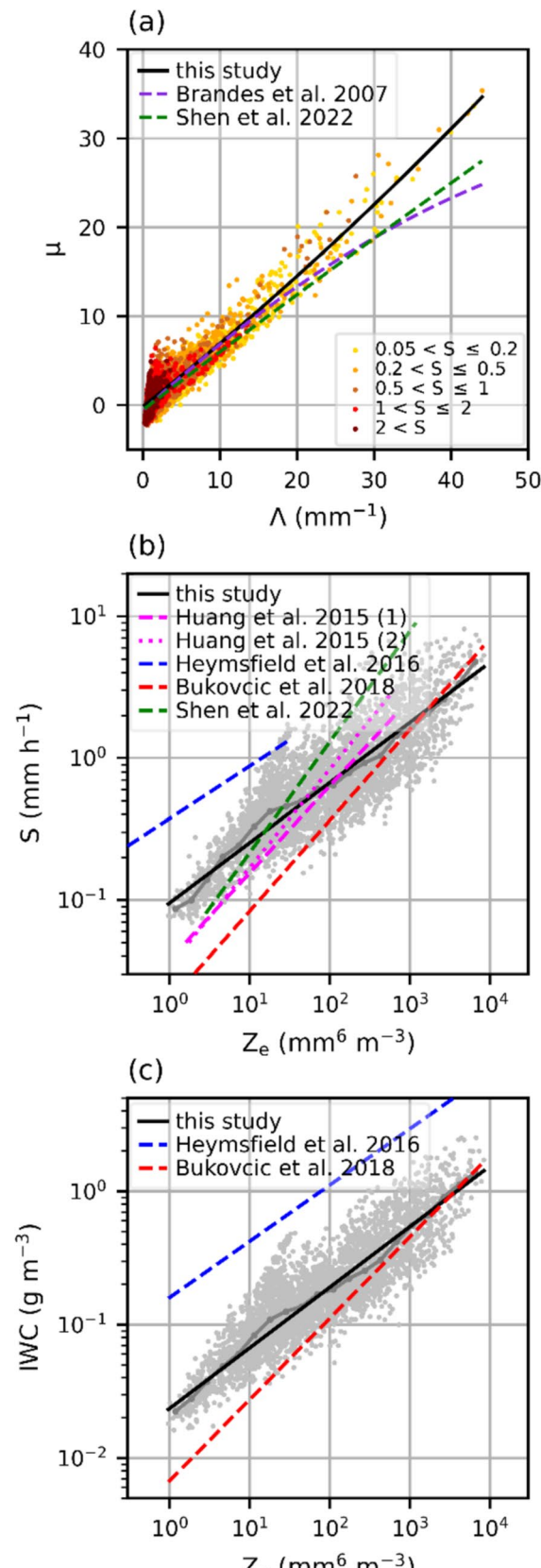


Table 1 Empirical $\Lambda-\mu$, Z_e-S , and Z_e-IWC relations in Fig. 10. For the convenience of comparison, all Z_e-S and Z_e-IWC relations are written in the forms of $S=aZ_e^b$ and $IWC=cZ_e^d$

Studies	Fitted relations
this study	$\mu=0.002\Lambda^2+0.685\Lambda-0.174$ $S=0.095 Z_e^{0.42}$ $IWC=0.023 Z_e^{0.45}$
Brandes et al. (2007)	$\mu=-0.005\Lambda^2+0.798\Lambda-0.666$
Huang et al. (2015)	(1) $S=0.038 Z_e^{0.61}$, (2) $S=0.034 Z_e^{0.69}$
Heymsfield et al. (2016)	$S=0.373 Z_e^{0.37}$ $IWC=0.159 Z_e^{0.42}$
Bukovčić et al. (2018)	$S=0.019 Z_e^{0.64}$ $IWC=0.0067 Z_e^{0.61}$
Shen et al. (2022)	$\mu=-0.0005\Lambda^2+0.658\Lambda-0.558$ $S=0.035 Z_e^{0.78}$

(COLD) and that for higher low-level temperatures (WARM) are selected and compared. The COLD snowfall has a wider PSD and less-rimed snow particles than the WARM snowfall. Due to the stronger northwesterlies, the meteorological conditions associated with the COLD snowfall exhibit relatively large vertical wind shear, small static (thermal) stability, low temperatures of -21 to -9 °C, and low humidity in the lower troposphere. These conditions suggest that enhanced aggregation by stronger turbulence and dendritic growths can contribute to the wider PSD and that weakened riming by shortages of supercooled liquid water for the lower temperatures might be associated with the less-rimed snow particles for the COLD snowfall. This result contributes to our understanding of relationships between meteorological conditions and snow characteristics which could be important for appropriate predictions and the precautions of snow-related damages in Seoul.

The disdrometer data used in this study show the characteristics of near-surface snow particles which offer valuable information as the product of all involved microphysical processes. However, they do not show the detailed sequence of individual microphysical processes that ice particles had experienced inside the precipitation systems aloft. Radar observations can complement the limitation of disdrometer data by providing the temporal evolution of the vertical profiles of microphysical characteristics, as shown by previous studies (e.g., Kim et al. 2021; Kulie et al. 2021). Future studies combining radar and disdrometer observations could further enhance our understanding of microphysical processes associated with snowfall in Seoul. In addition to the microphysical aspects examined in this study, the dynamical aspects of snowfall systems change with meteorological conditions. Numerical simulations can be a good option to examine the changes in both microphysical and dynamical aspects with environmental conditions. Further investigation using numerical simulations of sea-effect snowfall with

different strengths of cold and dry advection can help to comprehensively understand the snowfall changes associated with the expansion of the Siberian high in this region. Given that the winter climate of South Korea is expected to change along with climate change (Suh et al. 2016; Hong et al. 2017), understanding the impacts of climate change on snowfall characteristics in Seoul could be also important, which necessitates future investigation.

Acknowledgements We thank two anonymous reviewers for providing valuable comments on this work. This work was supported by the National Research Foundation of Korea (NRF) under grant 2021R1A2C1007044.

Declarations

Conflict of Interest The authors declare that they have no conflict of interest.

References

- Adhikari, A., Liu, C., Kulie, M.S.: Global distribution of snow precipitation features and their properties from 3 years of GPM observations. *J. Clim.* **31**, 3731–3754 (2018)
- Ahn, S.-H., Park, K.-J., Kim, J.-Y., Kim, B.-J.: The characteristics of the frequency and damage for meteorological disasters in Korea. *J. Korean Soc. Hazard Mitig.* **15**, 133–144 (2015). (in Korean with English abstract)
- Aikins, J., Friedrich, K., Geerts, B., Pokharel, B.: Role of a cross-barrier jet and turbulence on winter orographic snowfall. *Mon. Weather Rev.* **144**, 3277–3300 (2016)
- Allabakash, S., Lim, S., Chandrasekar, V., Min, K.H., Choi, J., Jang, B.: X-band dual-polarization radar observations of snow growth processes of a severe winter storm: Case of 12 December 2013 in South Korea. *J. Atmos. Ocean. Technol.* **36**, 1217–1235 (2019)
- Atkinson, B.W., Zhang, J.W.: Mesoscale shallow convection in the atmosphere. *Rev. Geophys.* **34**, 403–431 (1996)
- Atlas, D., Srivastava, R.C., Sekhon, R.S.: Doppler radar characteristics of precipitation at vertical incidence. *Rev. Geophys. Space Phys.* **2**, 1–35 (1973)
- Bao, B., Ren, G.: Sea-effect precipitation over the Shandong Peninsula, northern China. *J. Appl. Meteorol. Climatol.* **57**, 1291–1308 (2018)
- Bardal, K.G., Jørgensen, F.: Valuing the risk and social costs of road traffic accidents – Seasonal variation and the significance of delay costs. *Transp. Policy* **57**, 10–19 (2017)
- Barthold, F.E., Kristovich, D.A.R.: Observations of the cross-lake cloud and snow evolution in a lake-effect snow event. *Mon. Weather Rev.* **139**, 2386–2398 (2011)
- Brandes, E.A., Ikeda, K., Zhang, G., Schönhuber, M., Rasmussen, R.M.: A statistical and physical description of hydrometeor distributions in Colorado snowstorms using a video disdrometer. *J. Appl. Meteorol. Climatol.* **46**, 634–650 (2007)
- Brandes, E.A., Ikeda, K., Thompson, G., Schönhuber, M.: Aggregate terminal velocity/temperature relations. *J. Appl. Meteorol. Climatol.* **47**, 2729–2736 (2008)
- Bukovčić, P., Ryzhkov, A., Zrnić, D., Zhang, G.: Polarimetric radar relations for quantification of snow based on disdrometer data. *J. Appl. Meteorol. Climatol.* **57**, 103–120 (2018)
- Cao, Q., Zhang, G.: Errors in estimating raindrop size distribution parameters employing disdrometer and simulated raindrop spectra. *J. Appl. Meteorol. Climatol.* **48**, 406–425 (2009)



- Cerrai, D., Koukoula, M., Watson, P., Anagnostou, E.N.: Outage prediction models for snow and ice storms. *Sustain. Energy Grids Netw.* **21**, 100294 (2020)
- Cha, E.-J.: The state and socio-economic significance of the heavy snowfall in the Seoul metropolitan area on January 4, 2010. *Mag. Korean Soc. Hazard Mitig.* **10**, 6–13 (2010). (in Korean)
- Cha, J.W., Yum, S.S.: Characteristics of precipitation particles measured by PARISVEL disdrometer at a mountain and a coastal site in Korea. *Asia-Pac. J. Atmos. Sci.* **57**, 261–276 (2021)
- Cheong, S.-H., Byun, K.-Y., Lee, T.-Y.: Classification of snowfalls over the Korean Peninsula based on developing mechanism. *Atmosphere* **16**, 33–48 (2006). (in Korean with English abstract)
- Gehring, J., Oertel, A., Vignon, É., Jullien, N., Besic, N., Berne, A.: Microphysics and dynamics of snowfall associated with a warm conveyor belt over Korea. *Atmos. Chem. Phys.* **20**, 7373–7392 (2020)
- Gordon, G.L., Marwitz, J.D.: An airborne comparison of three PMS probes. *J. Atmos. Ocean. Technol.* **1**, 22–27 (1984)
- Ha, C.-H., Nam, Y.-M., Park, S.-K., Yuk, M.-R.: A study on the conditions for heavy snowfalls (over 5 cm) in Seoul. *Atmosphere* **11**, 185–187 (2001). (in Korean)
- Ha, K.-J., Heo, K.-Y., Lee, S.-S., Yun, K.-S., Jhun, J.-G.: Variability in the East Asian Monsoon: A review. *Meteorol. Appl.* **19**, 200–215 (2012)
- Hersbach, H., Bell, B., Berrisford, P., Hirahara, S., Horányi, A., Muñoz-Sabater, J., Nicolas, J., Peubey, C., Radu, R., Schepers, D., Simmons, A., Soci, C., Abdalla, S., Abellán, X., Balsamo, G., Bechtold, P., Biavati, G., Bidlot, J., Bonavita, M., Chiara, G.D., Dahlgren, P., Dee, D., Diamantakis, M., Dragani, R., Flemming, J., Forbes, R., Fuentes, M., Geer, A., Haimberger, L., Healy, S., Hogan, R.J., Hólm, E., Janisková, M., Keeley, S., Laloyaux, P., Lopez, P., Lupu, C., Radnoti, G., Rosnay, P.D., Rozum, I., Vamborg, F., Villaume, S., Thépaut, J.-N.: The ERA5 global reanalysis. *Q. J. R. Meteorol. Soc.* **146**, 1999–2049 (2020)
- Heymsfield, A.J.: A comparative study of the rates of development of potential graupel and hail embryos in High Plains storms. *J. Atmos. Sci.* **39**, 2867–2897 (1982)
- Heymsfield, A.J., Matrosov, S.Y., Wood, N.B.: Toward improving ice water content and snow-rate retrievals from radars. Part I: X and W bands, emphasizing CloudSat. *J. Appl. Meteorol. Climatol.* **55**, 2063–2090 (2016)
- Ho, C.-H., Kim, B.-G., Kim, B.-M., Park, D.-S.R., Park, C.K., Son, S.-W., Jeong, J.-H., Cha, D.-H.: Review of the weather hazard research: Focused on typhoon, heavy rain, drought, heat wave, cold surge, heavy snow, and strong gust. *Atmosphere* **33**, 223–246 (2023). (in Korean with English abstract)
- Hong, S.-Y., Dudhia, J., Chen, S.-H.: A revised approach to ice microphysical processes for the bulk parameterization of clouds and precipitation. *Mon. Weather Rev.* **132**, 103–120 (2004)
- Hong, J.-Y., Ahn, J.-B., Jhun, J.-G.: Winter climate changes over East Asian region under RCP scenarios using East Asian winter monsoon indices. *Clim. Dyn.* **48**, 577–595 (2017)
- Huang, G.-J., Bringi, V.N., Moisseev, D., Petersen, W.A., Bliven, L., Hudak, D.: Use of 2D-video disdrometer to derive mean density-size and Z_e -SR relations: Four snow cases from the light precipitation validation experiment. *Atmos. Res.* **153**, 34–48 (2015)
- Jeong, J., Park, R.: A study of the effects of SST deviations on heavy snowfall over the Yellow Sea. *Atmosphere* **23**, 161–169 (2013). (in Korean with English abstract)
- Kang, S.-D.: A case study on the mechanism of snowfall around Seoul region. *Atmosphere* **11**, 360–365 (2001)
- Kang, J.-Y., Kwon, Y.C.: Impacts of air-sea exchange coefficients on snowfall events over the Korean Peninsula. *J. Atmos. Sol.-Terr. Phys.* **146**, 1–15 (2016)
- Kim, K., Bang, W., Chang, E.-C., Tapiador, F.J., Tsai, C.-L., Jung, E., Lee, G.: Impact of wind pattern and complex topography on snow microphysics during International Collaborative Experiment for PyeongChang 2018 Olympic and Paralympic winter games (ICE-POP 2018). *Atmos. Chem. Phys.* **21**, 11955–11978 (2021)
- KMA: Climate average of South Korea. <https://data.kma.go.kr> (2024). Accessed 13 May 2024
- Kneifel, S., Moisseev, D.: Long-term statistics of riming in nonconvective clouds derived from ground-based Doppler cloud radar observations. *J. Atmos. Sci.* **77**, 3495–3508 (2020)
- Korolev, A.V., Isaac, G.A., Cober, S.G., Strapp, J.W., Hallett, J.: Microphysical characterization of mixed-phase clouds. *Q. J. R. Meteorol. Soc.* **129**, 39–65 (2003)
- KOSIS: Population. <https://kosis.kr> (2024). Accessed 13 May 2024
- Kulie, M.S., Milani, L.: Seasonal variability of shallow cumuliform snowfall: A CloudSat perspective. *Q. J. R. Meteorol. Soc.* **144**, 329–343 (2018)
- Kulie, M.S., Milani, L., Wood, N.B., Tushaus, S.A., Bennartz, R., L'Ecuyer, T.S.: A shallow cumuliform snowfall census using spaceborne radar. *J. Hydrometeorol.* **17**, 1261–1279 (2016)
- Kulie, M.S., Pettersen, C., Merrelli, A.J., Wagner, T.J., Wood, N.B., Dutter, M., Beachler, D., Kluber, T., Turner, R., Mateling, M., Lenters, J., Blanken, P., Maahn, M., Spence, C., Kneifel, S., Kucera, P.A., Tokay, A., Bliven, L.F., Wolff, D.B., Petersen, W.A.: Snowfall in the northern Great Lakes: Lessons learned from a multisensor observatory. *Bull. Am. Meteorol. Soc.* **102**, E1317–E1339 (2021)
- Kusunoki, K., Murakami, M., Orikasa, N., Hoshimoto, M., Tanaka, Y., Yamada, Y., Mizuno, H., Hamazu, K., Watanabe, H.: Observations of quasi-stationary and shallow orographic snow clouds: Spatial distributions of supercooled liquid water and snow particles. *Mon. Weather Rev.* **133**, 743–751 (2005)
- Lee, I.-Y.: Examination of phenomena preceding heavy snowfalls in the northern Gyeonggi region. *Atmosphere* **12**, 352–357 (2002a). (in Korean)
- Lee, W.-G.: Winter heavy snowfall forecasting techniques in the Seoul and Gyeonggi regions. *Atmosphere* **12**, 124–125 (2002b). (in Korean)
- Lee, J.-G., Min, K.-H.: Analysis of the west coast heavy snowfall development mechanism from 23 to 25 January 2016. *Atmosphere* **28**, 53–67 (2018). (in Korean with English abstract)
- Lee, W.-K., Lee, H.-A., Hwang, S.-S., Kim, H., Lim, Y.-H., Hong, Y.-C., Ha, E.-H., Park, H.: Does temperature modify the effects of rain and snow precipitation on road traffic injuries? *J. Epidemiol.* **25**, 544–552 (2015)
- Lee, J., Jin, H.-G., Baik, J.-J.: Regional differences in raindrop size distribution observed from disdrometers in South Korea and their possible causes. *Theor. Appl. Climatol.* **150**, 847–862 (2022)
- Liao, L., Meneghini, R., Tokay, A.: Uncertainties of GPM DPR rain estimates caused by DSD parameterizations. *J. Appl. Meteorol. Climatol.* **53**, 2524–2537 (2014)
- Libbrecht, K.G.: The physics of snow crystals. *Rep. Prog. Phys.* **68**, 855–895 (2005)
- Locatelli, J.D., Hobbs, P.V.: Fall speeds and masses of solid precipitation particles. *J. Geophys. Res.* **79**, 2185–2197 (1974)
- Löffler-Mang, M., Blahak, U.: Estimation of the equivalent radar reflectivity factor from measured snow size spectra. *J. Appl. Meteorol.* **40**, 843–849 (2001)
- Markowski, P., Richardson, Y.: Mesoscale Meteorology in Midlatitudes. Wiley-Blackwell, West Sussex (2010)
- Mazon, J., Niemelä, S., Pino, D., Savijärvi, H., Vihma, T.: Snow bands over the Gulf of Finland in wintertime. *Tellus A: Dyn. Meteorol. Oceanogr.* **67**, 25102 (2015)
- MOIS: 2022 Disaster Annual Report. Ministry of the Interior and Safety, Sejong City (2024)
- Morrison, H., Thompson, G., Tatarskii, V.: Impact of cloud microphysics on the development of trailing stratiform precipitation

- in a simulated squall line: Comparison of one- and two-moment schemes. *Mon. Weather Rev.* **137**, 991–1007 (2009)
- Nakai, S., Iwanami, K., Misumi, R., Park, S.-G., Kobayashi, T.: A classification of snow clouds by Doppler radar observations at Nagaoka, Japan. *SOLA* **1**, 161–164 (2005)
- Nam, H.-G., Kim, B.-G., Han, S.-O., Lee, C., Lee, S.-S.: Characteristics of easterly-induced snowfall in Yeongdong and its relationship to air-sea temperature difference. *Asia-Pac. J. Atmos. Sci.* **50**, 541–552 (2014)
- NBSC: Statistical communiqué of the people's republic of China on the 2022 national economic and social development. https://www.stats.gov.cn/english/PressRelease/202302/t20230227_1918979.html (2023). Accessed 10 May 2024
- NCEI: Billion-dollar weather and climate disasters. <https://www.ncei.noaa.gov/access/billions/> (2024). Accessed 10 May 2024
- Nešpor, V., Krajewski, W.F., Kruger, A.: Wind-induced error of raindrop size distribution measurement using a two-dimensional video disdrometer. *J. Atmos. Ocean. Technol.* **17**, 1483–1492 (2000)
- Niziol, T.A.: Operational forecasting of lake effect snowfall in western and central New York. *Weather Forecast.* **2**, 310–321 (1987)
- Niziol, T.A., Snyder, W.R., Waldstreicher, J.S.: Winter weather forecasting throughout the eastern United States. Part IV: Lake effect snow. *Weather Forecast.* **10**, 61–77 (1995)
- Noguchi, T., Fujii, T.: Minimizing the effect of natural disasters. *Jpn. Railw. Transp. Rev.* **23**, 52–59 (2000)
- Norris, J., Vaughan, G., Schultz, D.M.: Snowbands over the English Channel and Irish Sea during cold-air outbreaks. *Q. J. R. Meteorol. Soc.* **139**, 1747–1761 (2013)
- Pettersen, C., Kulie, M.S., Bliven, L.F., Merrelli, A.J., Petersen, W.A., Wagner, T.J., Wolff, D.B., Wood, N.B.: A composite analysis of snowfall modes from four winter seasons in Marquette, Michigan. *J. Appl. Meteorol. Climatol.* **59**, 103–124 (2020)
- Pinsky, M.B., Khain, A.P.: Some effects of cloud turbulence on water–ice and ice–ice collisions. *Atmos. Res.* **47–48**, 69–86 (1998)
- Pinsky, M., Khain, A., Korolev, A.: Phase transformations in an ascending adiabatic mixed-phase cloud volume. *J. Geophys. Res.: Atmos.* **120**, 3329–3353 (2015)
- Pu, K., Liu, X., He, H., Sun, Y., Hu, S., Wu, Y.: Microphysical characteristics of winter precipitation in eastern China from 2014 to 2019. *Water* **12**, 920 (2020)
- Rauber, R.M.: Characteristics of cloud ice and precipitation during wintertime storms over the mountains of northern Colorado. *J. Clim. Appl. Meteorol.* **26**, 488–524 (1987)
- RWMP: How do weather events impact roads? https://ops.fhwa.dot.gov/weather/q1_roadimpact.htm (2023). Accessed 10 May 2024
- Seifert, A., Leinonen, J., Siewert, C., Kneifel, S.: The geometry of rimed aggregate snowflakes: A modeling study. *J. Adv. Model. Earth Syst.* **11**, 712–731 (2019)
- Shen, Y., Chen, Y., Bi, Y., Lyu, D., Chen, H., Duan, S.: Snowfall microphysics characterized by PARASIVE disdrometer observations in Beijing from 2020 to 2022. *Remote Sens.* **14**, 6025 (2022)
- Shijin, W., Yuande, Y., Yanjun, C.: Global snow- and ice-related disaster risk: A review. *Nat. Hazards Rev.* **23**, 03122002 (2022)
- Son, Y.T., Lee, S.H., Im, J.H.: A study on highway capacity variation according to snowfall intensity. *J. Korean Soc. Transp.* **31**, 3–11 (2013). (in Korean with English abstract)
- Souto, L., Neal, R., Pope, J.O., Gonzalez, P.L.M., Wilkinson, J., Taylor, P.C.: Identification of weather patterns and transitions likely to cause power outages in the United Kingdom. *Commun. Earth Environ.* **5**, 49 (2024)
- Steenburgh, W.J., Nakai, S.: Perspectives on sea- and lake-effect precipitation from Japan's "Gosetsu Chitai". *Bull. Am. Meteorol. Soc.* **101**, E58–E72 (2020)
- Stewart, R.E., Bachand, D., Dunkley, R.R., Giles, A.C., Lawson, B., Legal, L., Miller, S.T., Murphy, B.P., Parker, M.N., Paruk, B.J., Yau, M.K.: Winter storms over Canada. *Atmos.-Ocean* **33**, 223–247 (1995)
- Strauss, L., Serafin, S., Dorninger, M.: Skill and potential economic value of forecasts of ice accretion on wind turbines. *J. Appl. Meteorol. Climatol.* **59**, 1845–1864 (2020)
- Suh, M.-S., Oh, S.-G., Lee, Y.-S., Ahn, J.-B., Cha, D.-H., Lee, D.-K., Hong, S.-Y., Min, S.-K., Park, S.-C., Kang, H.-S.: Projections of high resolution climate changes for South Korea using multiple-regional climate models based on four RCP scenarios. Part 1: Surface air temperature. *Asia-Pac. J. Atmos. Sci.* **52**, 151–169 (2016)
- Tao, R., Zhao, K., Huang, H., Wen, L., Zhang, G., Zhou, A., Chen, H.: Snow particle size distribution from a 2-D video disdrometer and radar snowfall estimation in East China. *IEEE Trans. Geosci. Remote Sens.* **59**, 196–207 (2021)
- Taszarek, M., Kendzierski, S., Pilgj, N.: Hazardous weather affecting European airports: Climatological estimates of situations with limited visibility, thunderstorm, low-level wind shear and snowfall from ERA5. *Weather Clim. Extrem.* **28**, 100243 (2020)
- Thompson, E.J., Rutledge, S.A., Dolan, B., Thurair, M.: Drop size distributions and radar observations of convective and stratiform rain over the equatorial Indian and west Pacific Oceans. *J. Atmos. Sci.* **72**, 4091–4125 (2015)
- Tokay, A., Wolff, D.B., Petersen, W.A.: Evaluation of the new version of the laser-optical disdrometer, OTT Parsivel². *J. Atmos. Ocean. Technol.* **31**, 1276–1288 (2014)
- Vivekanandan, J., Zhang, G., Brandes, E.: Polarimetric radar estimators based on a constrained gamma drop size distribution model. *J. Appl. Meteorol.* **43**, 217–230 (2004)
- Wang, L., Chen, Z., Zhang, W., Lu, Z., Cheng, Y., Qu, X., Gul, C., Yang, Y.: The causes and forecasting of icing events on power transmission lines in southern China: A review and perspective. *Atmosphere* **14**, 1815 (2023)
- Yu, D.-B., Kim, K.-E.: Analysis of kinematic characteristics of snow clouds and development of cloud street by Doppler radar observation. *J. Korean Meteorol. Soc.* **41**, 877–896 (2005). (in Korean with English abstract)
- Yu, T., Chandrasekar, V., Xiao, H., Joshi, S.S.: Characteristics of snow particle size distribution in the PyeongChang region of South Korea. *Atmosphere* **11**, 1093 (2020)
- Zhang, G., Vivekanandan, J., Brandes, E.: A method for estimating rain rate and drop size distribution from polarimetric radar measurements. *IEEE Trans. Geosci. Remote Sens.* **39**, 830–841 (2001)
- Zhang, G., Xue, M., Cao, Q., Dawson, D.: Diagnosing the intercept parameter for exponential raindrop size distribution based on video disdrometer observations: Model development. *J. Appl. Meteorol. Climatol.* **47**, 2983–2992 (2008)
- Zhang, G., Luchs, S., Ryzhkov, A., Xue, M., Ryzhkova, L., Cao, Q.: Winter precipitation microphysics characterized by polarimetric radar and video disdrometer observations in central Oklahoma. *J. Appl. Meteorol. Climatol.* **50**, 1558–1570 (2011)

Publisher's Note Springer Nature remains neutral with regard to jurisdictional claims in published maps and institutional affiliations.

Springer Nature or its licensor (e.g. a society or other partner) holds exclusive rights to this article under a publishing agreement with the author(s) or other rightsholder(s); author self-archiving of the accepted manuscript version of this article is solely governed by the terms of such publishing agreement and applicable law.